ACS OMEGA

Open Access

http://pubs.acs.org/journal/acsodf

Article

The Influence of Synthetic Parameters on HgSe QDs

Suhui Wang, Tengxiao Guo,* and Shuya Cao*

Cite This: *ACS Omega* 2023, 8, 44804−44811

Read Online

ACCESS | Metrics & More | Article Recommendations | Supporting Information

ABSTRACT: HgSe quantum dots (QDs) were synthesized by a thermal injection method. The effects of material ratio, growth time, and reaction temperature on the growth and spectral properties of the QDs have been studied. The experimental results show that the QDs had the highest yield of 53.04% when the molar ratio of Se source to Hg source was 1.5. Also, the excess source of SeS_2 was reduced to Se. In addition, the critical radius and spectral red-shift rate of QDs can be increased with the reaction temperature. When the reaction temperature was increased to 100 °C, the spectrum reached far-infrared and the growth rate was increased to 10 times and reached 0.63 nm/min. Differing particle morphologies can be obtained by increasing the growth time to 40 min. Moreover, the growth rate reached the minimum at 30 min and the maximum at 80 min of the growth time. This study can provide guidance for the synthesis of long-wave infrared QD materials.

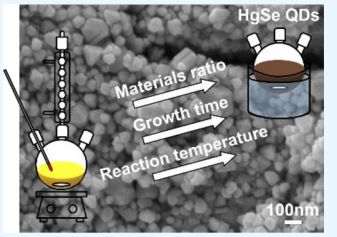

1. INTRODUCTION

There have been numerous methods developed for the synthesis of semiconductor QDs over the past decade. Among them, the absorption spectrum of HgSe QDs can reach more than 14 μm. It was one of the excellent building blocks to develop low-cost infrared (IR) optoelectronic devices. Although the use of compounds containing mercury (such as mercuric sulfide (HgS), mercuric oxide (HgO), mercuric chloride ($HgCl_2$), and mercurous chloride (Hg_2Cl_2)) was limiting due to them being extremely toxic and expensive, it was still sought after by researchers as the materials were easy to prepare and tunable across the IR spectrum when prepared as nanoparticles of various sizes.

Howes et al. first proposed the use of an organic synthesis to prepare HgSe QDs. Mercury acetate ($Hg(OAc)_2$), trioctylphosphine oxide (TOPO), ethanol, and selenium powder were used as raw materials. The mean diameter was 4.9 nm, the exciton characteristics were below 1 μm, and no fluorescence was observed.[1] Deng et al. prepared HgSe QDs with sizes of 5.5, 5.9, and 6.2 nm and absorption bands of 3−5 μm; the red-shift phenomenon was observed as the growth time increased, laying a material synthesis basis for the preparation of midwave infrared (MWIR) detectors of QDs.[2] In 2016, the team grew a single-layer CdS shell on the basis of bare core HgSe QDs, which effectively improved the in-band luminescence of HgSe QDs and enhanced the chemical and thermal stability.[3] Lhuillier and Scarafagio prepared HgSe QDs based on the organic synthesis method. HgSe QDs with sizes ranging from 8 to 9.6 nm were obtained, and their in-band characteristic absorption extends to the terahertz band, covering an extremely wide wavelength range of 3−20 μm.[4] This method was of great significance for the preparation of low-cost MWIR and FWIR detectors operating at room temperature.

However, most of the reports about HgSe QDs focus on the research of synthesis methods or the preparation of devices,[5−10] and there was no detailed research on the influence of synthesis parameters on the HgSe QDs. Herein, we reported the effects of experimental parameters such as raw material ratio, growth time, and reaction temperature on the growth and spectral characteristics of HgSe QDs. This is of great significance for material synthesis and device fabrication.

2. EXPERIMENTAL CONTENT

2.1. Chemicals. Mercuric acetate ($Hg(OAc)_2$, 99.5%), oleylamine (OAm, 70%), oleic acid (OAc), selenium disulfide (SeS_2, 99.99%), and toluene (98%) were purchased from Acmec. Ethanol (99.5%), tetrachloroethylene (PCE, 98%), and *n*-hexane (98%) were purchased from Macklin. All chemicals were used as received.

2.2. System. First, a water and oxygen free system (Schlenk Line) was constructed. Then, the four-necked flask and measuring cylinder were cleaned with dishwashing liquid, ethanol, acetone, and deionized water by sonicating for 15 min to remove impurities and solvents. Next, the utensils were dried at 100 °C. Finally, the flask was attached to the system.

2.3. Synthesis of HgSe QDs with Different Ratios of Precursor. $Hg(OAc)_2$ (2.2 g) was dissolved in 80 mL of OAm and 40 mL of OAc in the flask. The flask was degassed under vacuum for 10 min at 80 °C. The atmosphere was switched to N_2; meanwhile, Se precursor solution was prepared by sonicating 1, 1.5, 2, and 4 g of SeS_2 powder in 30 mL of OAm, respectively. Then, the Se precursor with different ratios was quickly injected into the flask, and the solution turned dark.

Received: August 11, 2023
Revised: October 25, 2023
Accepted: October 27, 2023
Published: November 14, 2023

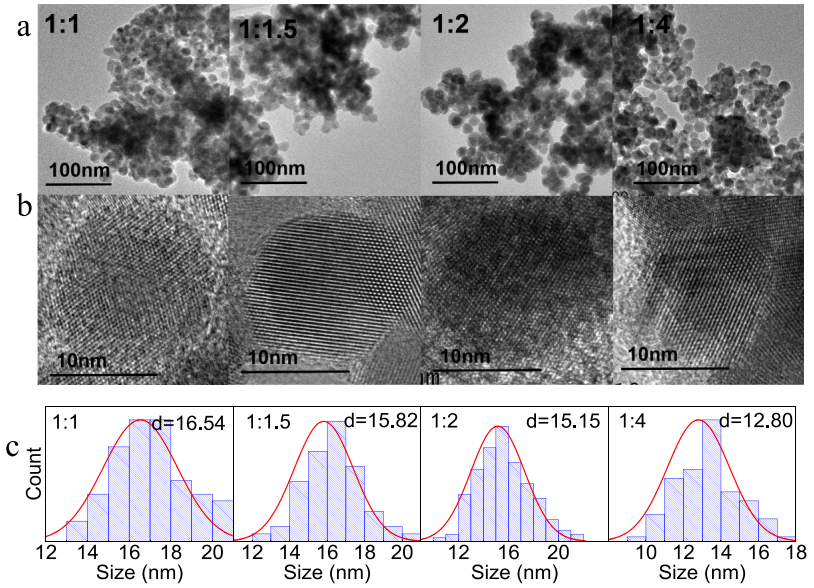

Figure 1. (a) TEM characterization; (b) crystal lattice; (c) size of HgSe QDs synthesized when the ratios of $Hg(OAc)_2$ to SeS_2 were 1:1, 1:1.5, 1:2, and 1:4.

The reaction was continued for 10 min before being quenched by addition of 40 mL of *n*-hexane. The solution was mixed with the triple volume of ethanol and centrifuged for 10 min at 7000 rpm. After that, the supernatant was decanted, and the precipitate was mixed with 5 mL of toluene and 15 mL of ethanol and centrifuged at 7000 rpm for 10 min, repeated twice. The obtained solid was dried for 24 h and dissolved in PCE.

2.4. Synthesis of HgSe QDs with Different Growth Times and Reaction Temperatures. $Hg(OAc)_2$ (2.2 g) was dissolved in 80 mL of OAm and 40 mL of OAc in the flask. The flask was degassed under vacuum for 10 min at 60, 80, and 100 °C, respectively. The atmosphere was switched to N_2; meanwhile, Se precursor solution was prepared by sonicating 1.5 g of SeS_2 powder in 30 mL of OAm. Then, the mixture was quickly injected into the flask, and the solution turned dark. The reaction was continued for 10−90 min (samples were taken every 10 min) before being quenched by addition of 5 mL of *n*-hexane. The solution was mixed with the triple volume of ethanol and centrifuged for 10 min at 7000 rpm. After that, the supernatant was decanted, the precipitate was mixed with 5 mL of toluene and 15 mL of ethanol, and centrifuged at 7000 rpm for 10 min, repeated twice. The obtained solid was dried for 24 h and dissolved in PCE.

2.5. Characterization of HgSe QDs. *2.5.1. Transmission Electron Microscopy.* The solution of HgSe QDs was dropcasted on copper and degassed under vacuum. The TEM images were obtained from a JEM-F200 (JEOL, Japan) at 170 kV.

2.5.2. Spherical Aberration Transmission Electron Microscopy−X-ray Energy Dispersive Spectroscopy. STEM images were obtained on a FEI Theims Z (Thermo Scientific, USA) with a copper grid using an accelerating voltage of 150 kV. The FEI Theims Z was equipped with an EDS with 20 kV accelerated voltage.

2.5.3. Scanning Electron Microscopy. A small amount of powder was taken and stuck directly onto the conductive adhesive, and 10 mA current was used for spraying gold to obtain the sample. The SEM images were obtained using a MIRA LMS (TESCAN, Czech) under 3 kV detection acceleration voltage.

2.5.4. X-ray Diffraction. The XRD analysis was carried out on the nanoparticle powders using a Smartlab-3KW+UltimalV3KW (Rigaku Corporation, Japan). The test target was copper, and the range was 20−80° at a speed of 4°/min.

2.5.5. Fourier Transform Infrared Spectroscopy. The IR transmission spectra were measured from an Alpha II spectrometer (Bruker, Germany) of potassium bromide tablet for HgSe QDs. The spectra were typically acquired between 2500 and 400 cm^{-1} with 4 cm^{-1} resolution and averaging over 32 spectra.

3. RESULTS AND DISCUSSION

3.1. Effect of Precursor Ratio on HgSe QDs. *3.1.1. The Characterization of TEM and STEM.* The TEM characterization and size of HgSe QDs synthesized with different ratios of materials are shown in Figure 1.

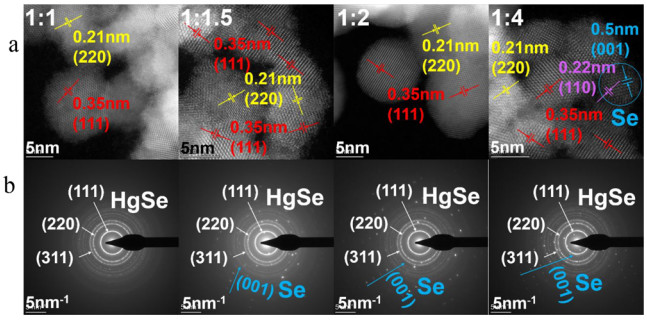

Figure 2. (a) STEM characterization; (b) SEAD pattern at the ratios of $Hg(OAc)_2$ to SeS_2 of 1:1, 1:1.5, 1:2, and 1:4.

As can be seen from Figure 1, spherical HgSe QD crystals can be obtained by synthesis with four material ratios of 1:1, 1:1.5, 1:2, and 1:4. The average particle size of QDs decreased gradually with the increase in SeS_2.[11]

In addition, the results of STEM (Figure 2a) and selected-area electron diffraction (SAED) (Figure 2b) indicated that the extra SeS_2 will be reduced to Se elemental substance when SeS_2 is excessive (the molar ratio of $Hg(OAc)_2$ and SeS_2 was greater

https://doi.org/10.1021/acsomega.3c05910
ACS Omega 2023, 8, 44804−44811

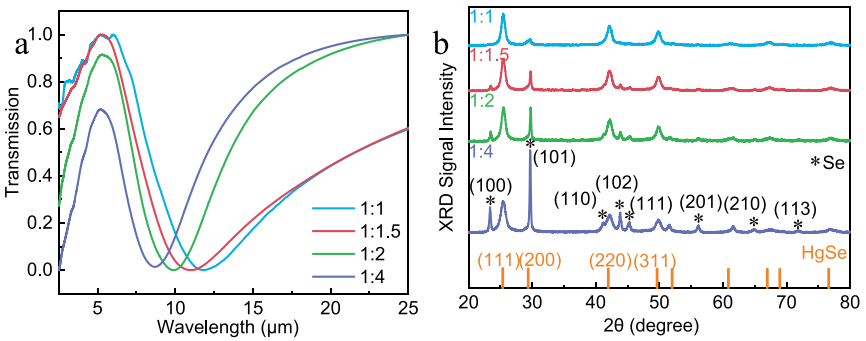

Figure 3. (a) Transmission spectra; (b) XRD of HgSe QDs synthesized when the ratios of $Hg(OAc)_2$ to SeS_2 were 1:1, 1:1.5, 1:2, and 1:4.

Table 1. Modified Value of the Se Elementary Substance and HgSe QDs and the Content of the HgSe QDs

$Hg(OAc)_2$:SeS_2 (mol)	calculated radius of Se after being modified (nm)	calculated radius of HgSe QDs after being modified (nm)	measured radius of the sample (nm)	content of HgSe QDs (%)
1:1		16.54	16.54	100
1:1.5	27.46	15.54	15.82	97.65
1:2	28.46	14.76	15.15	97.15
1:4	30.74	12.13	12.80	96.38

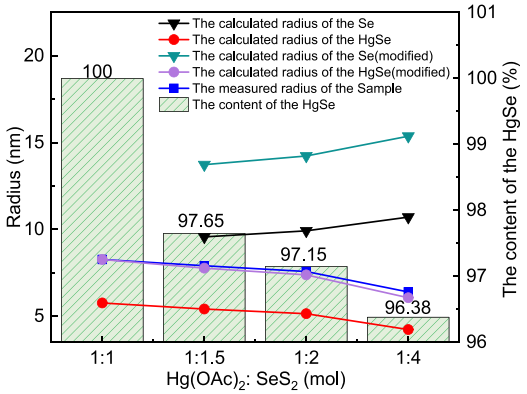

Figure 4. Modified value of Se elementary substance and HgSe QDs and the content of the HgSe QDs.

Table 2. Average Yield of HgSe QDs Synthesized with Different Material Ratios

$Hg(OAc)_2$:SeS_2 (mol)	1:1	1:1.5	1:2	1:4
total yield (%)	41.71	54.32	45.26	43.49
yield of HgSe QDs (%)	41.71	53.04	43.97	41.92

than 1:1). According to the diffraction spots, these selenium substances are single crystals growing in the (001) direction or the triangle phase *c* axis direction.[12−16]

Table 3. Elemental Content of Hg and Se in Products with Different Material Ratios

	weight (%)		atomic (%)	
$Hg(OAc)_2$: SeS_2 (mol)	Hg	Se	Hg	Se
1:1	71.95	28.05	50.24	49.76
1:1.5	71.89	28.11	50.17	49.83
1:2	69.65	30.35	47.46	52.54
1:4	66.74	33.26	44.13	55.87

However, the cause of the decrease in particle size was not clear; FTIR, XRD, and EDS were performed for further research.

3.1.2. The Characterization of FTIR and XRD. The FTIR and XRD characterizations of HgSe QDs are shown in Figure 3.

According to the result of FTIR, the transmission peak of HgSe QDs shifted blue with the increase in SeS_2 in the ratio of materials, and the particle size of QDs gradually decreased according to the quantum confinement effect, which was consistent with the TEM test results described above.

It can been known from Figure 3b that all of the HgSe QDs were zinc blende. The diffraction peak of Se elementary substance appeared (indicated by * in the figure) when the molar ratio of $Hg(OAc)_2$ to SeS_2 was greater than 1:1.[17−19]

The intensity and distribution of XRD were closely related to the particle size of the nanoparticles, which can usually be calculated by the Scherrer equation. As shown in formula 1:

$$D = \frac{K\lambda}{B\cos\theta} \quad (1)$$

where λ is the wavelength of X-ray, K is the form factor, the value range is 0.85−0.9, and spherical particles are generally 0.89. B is the half-peak width height of the response diffraction line, and θ is the Bragg angle in response to the diffraction line.

To eliminate the measurement errors from characterization and the approximation errors from the form factor, the reaction was assumed completely when the ratio of $Hg(OAc)_2$ to SeS_2 was 1:1 (the product was HgSe QDs). The calculated values were revised using the measured particle size of the sample. The

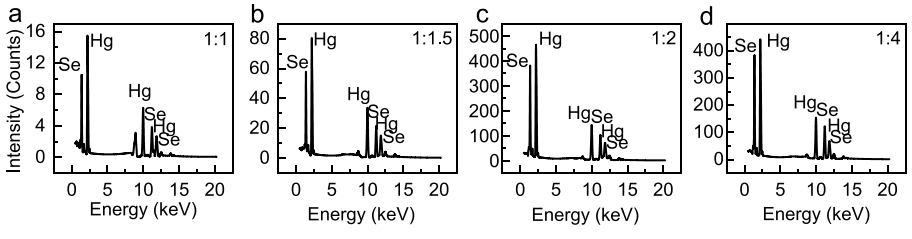

Figure 5. EDS energy spectrum of HgSe QDs synthesized when the ratios of $Hg(OAc)_2$ to SeS_2 were (a) 1:1, (b) 1:1.5, (c) 1:2, and (d) 1:4.

https://doi.org/10.1021/acsomega.3c05910
ACS Omega 2023, 8, 44804−44811

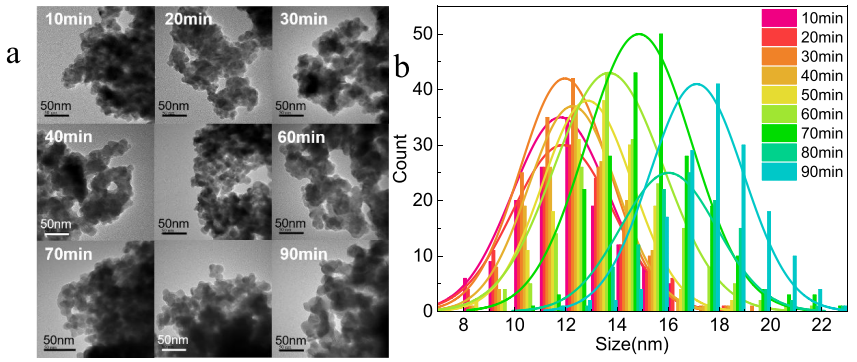

Figure 6. (a) TEM of HgSe QDs synthesized at a reaction temperature of 60 °C; (b) diameter of HgSe QDs.

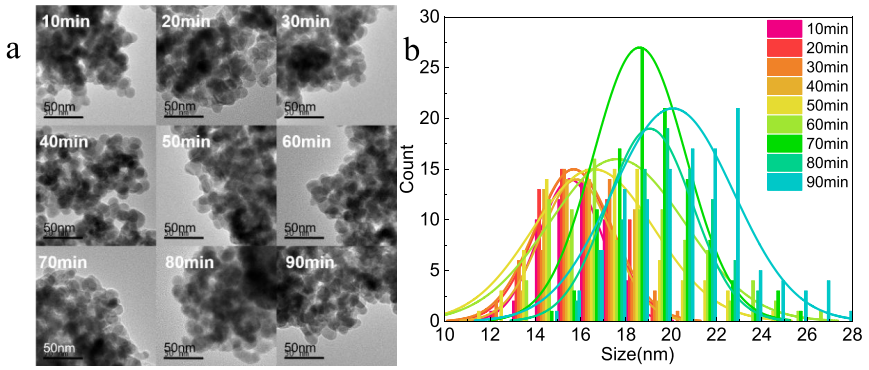

Figure 7. (a) TEM of HgSe QDs synthesized at a reaction temperature of 80 °C; (b) diameter of HgSe QDs.

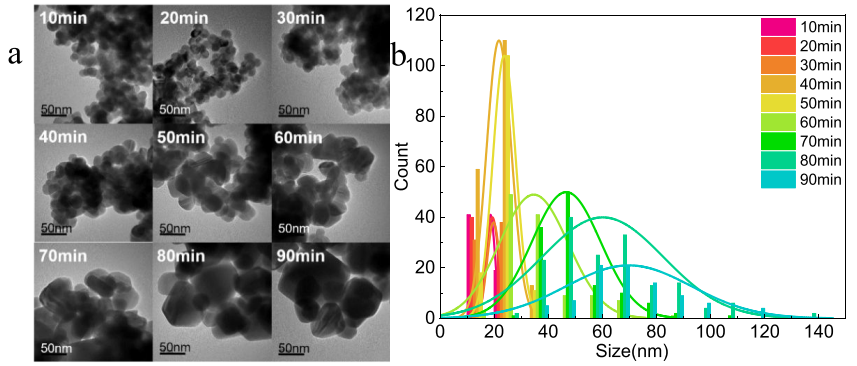

Figure 8. (a) TEM of HgSe QDs synthesized at a reaction temperature of 100 °C; (b) diameter of HgSe QDs.

original calculated values are shown in Table S1. The correction factor obtained by calculation was 1.434. The modified size of Se and HgSe QDs and the content of the HgSe QDs in the sample are shown in Table 1 and Figure 4.

It can be seen from Table 1 and Figure 4 that the modified radius of HgSe QDs consisted of the measured radius of the sample. The content of HgSe QDs was decreased, and the radius of Se was increased with the ratio of SeS_2. The average yield of HgSe QDs synthesized with different material ratios was calculated, as shown in Table 2. The results showed that the highest yield occurred when the molar ratio of $Hg(OAc)_2$ to SeS_2 was 1:1.5. Therefore, the subsequent experiments were carried out on the basis of this ratio.

3.1.3. The Characterization of EDS. The EDS energy spectrum of HgSe QDs is shown in Figure 5 (the elemental mapping of HgSe QDs is shown in Figure S1), and the normalized weight percentage content and normalized atomic percentage content of Hg and Se elements are shown in Table 3.

According to the EDS in Figure 5 and element content in Table 3, when the ratio of $Hg(OAc)_2$ to SeS_2 was 1:1, the normalized mass percentage content ratio of Hg to Se was 7:3, and the normalized atomic percentage content was 1:1, indicating that the reaction system was stable and the zinc blende structure was retained as the whole growth of HgSe QDs.

However, the content of Se in the product was increased with the ratio of SeS_2, which was related to the increased Se atom content in HgSe QDs or Se elemental substance. Since the atomic radius of Se was 1.22 Å and that of Hg was 1.76 Å, the average particle size of the product decreased gradually with the ratio of SeS_2, which was consistent with the conclusion of FTIR and XRD characterization above. In summary, the excessive amounts of SeS_2 will be reduced to the Se elemental substance. The particle size of the reduced Se element increased with the content of SeS_2. Since the growth of QDs is competitive with that of Se elements, too much SeS_2 is not conducive to the growth of HgSe QDs, and it leads to the decrease in the particle

https://doi.org/10.1021/acsomega.3c05910
ACS Omega 2023, 8, 44804−44811

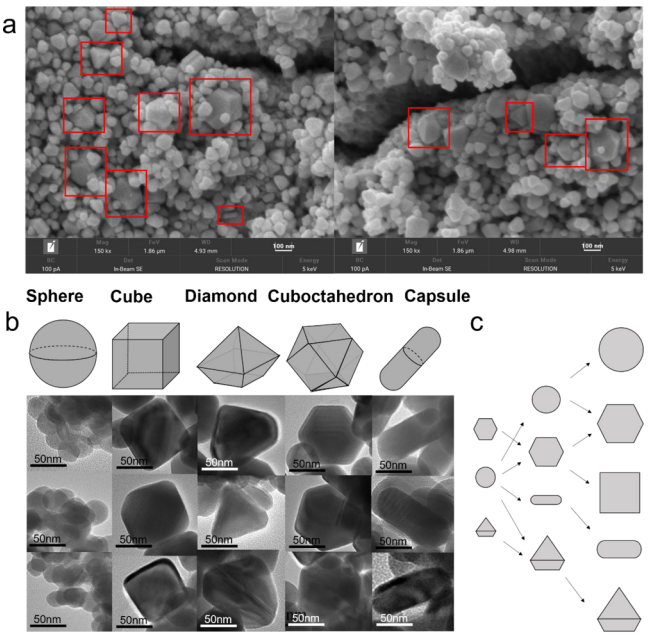

Figure 9. (a) SEM image of HgSe QDs synthesized at 100 °C and 90 min; (b) different shapes of HgSe QDs (TEM image); (c) growth process of the HgSe QDs.

size of HgSe QDs. In addition, the best raw material ratio (1:1.5) for HgSe QD synthesis was obtained to get the highest QD content and yield of the product.

3.2. Effect of Growth Time and Reaction Temperature on HgSe QDs. *3.2.1. The Characterization of TEM.* The TEM and diameter of HgSe QDs synthesized at different growth times and reaction temperatures are shown in Figure 6a,b (scale, 50 nm), Figure 7a,b (scale, 50 nm), and Figure 8a,b (scale, 50 nm), respectively. The original data of diameter are shown in Table S2 (Supporting Information).

As can be seen from Figures 6 and 8, the shape of HgSe QDs was spherical, and the average size of the QDs gradually increased with the growth time and reaction temperature when the reaction temperatures were 60 and 80 °C.

As can be seen from Figure 8, when the reaction temperature reached 100 °C, the HgSe QDs with the shapes of cube, diamond, cub octahedron, and capsule occurred after 40 min of growth, and the volume increased rapidly.

The shape of nanocrystals is controlled by two traditional methods: One is to change the passivation effect of different crystal planes of QDs by adjusting the surfactant. The second is to control the saturation rate of QDs with different crystal planes by adjusting the precursor concentration.

However, OAm and OAc were always used as surfactants with the concentration of precursors remaining, so the saturation degree and growth rate of different crystal planes can also be affected by the reaction temperature and growth time.

Both perovskite QDs and PbTe QDs can be transformed from cuboctahedron into cube.[20,21] Therefore, it was deduced that the shape of QDs was mostly spherical with a few cuboctahedron and diamond shapes by TEM. With the increased growth time and reaction temperature, these spherical HgSe nanocrystals began to change to cube, diamond, cuboctahedron, and capsule. The cuboctahedral QDs further grew or evolved into cube QDs. The diamond QDs kept growing in that shape, and the size distributions of all shapes of HgSe QDs became broader. The different shapes and the growth regular of HgSe QDs are shown in Figure 9a–c.

Some studies indicated that the particles would become more faceted but lose their narrow size distribution as the concentration of coordinating solvent in the reaction solution was reduced.[1] This was consistent with our experimental results; when the reaction temperature reached 100 °C, differing particle morphologies of HgSe QDs were obtained, and with the increase in growth time, a wider size distribution appeared (Figure S2c, Supporting Information). In the thermodynamically dominated growth system, spherical nanocrystals have the lowest surface energy and therefore serve as the first form of crystal growth; when the reaction temperature is raised, the adhesion and separation rate of ligands on the surface of nanocrystals is accelerated with the increase in reaction temperature, and atoms have more opportunities to grow on the crystal surface, forming a polyhedron with a thermodynamically stable surface.[22]

The relationship between the diameter and the growth time of HgSe QDs is shown in Figure S2 (Supporting Information). The relationship curves between the growth rate and the radius of HgSe QDs have been fitted, as shown in Figure 10.

The maximum growth rates of HgSe QDs synthesized at the reaction temperatures of 60, 80, and 100 °C were 0.06, 0.06, and 0.63 nm/min, and the critical radii of QDs were 7.91, 9.40, and 26.92 nm, respectively. Then, the HgSe QDs entered the "Ostwald Ripening" process, and the QDs with a radius less than the critical radius begin to dissolve. On the contrary, the QDs with a radius greater than the critical radius continue to grow, and the overall particle size distribution became wider, which is called "defocusing". The error bars in Figure S2 (Supporting Information) reflected the "defocusing" phenomenon.

According to the classical Lamer theory,[23,24] the concentration of monomers in the solution increased instantaneously when the two precursor solutions were quickly injected into the flask at high temperature, resulting in nuclear reaction, while the

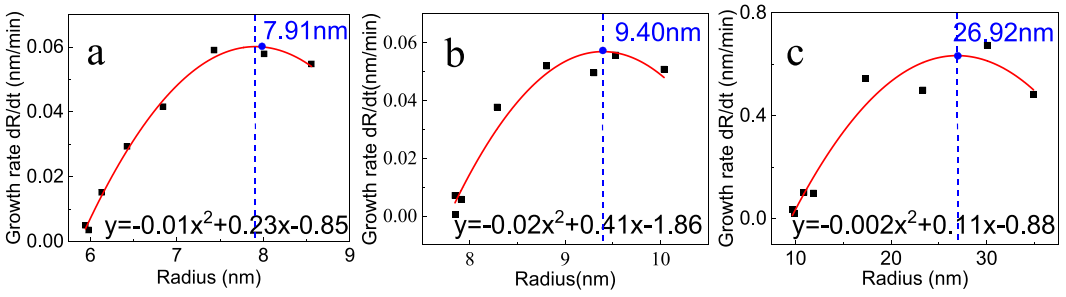

Figure 10. Relationship curves between the growth rate and the radius of HgSe QDs. (a) 60 °C; (b) 80 °C; (c) 100 °C.

https://doi.org/10.1021/acsomega.3c05910
ACS Omega 2023, 8, 44804−44811

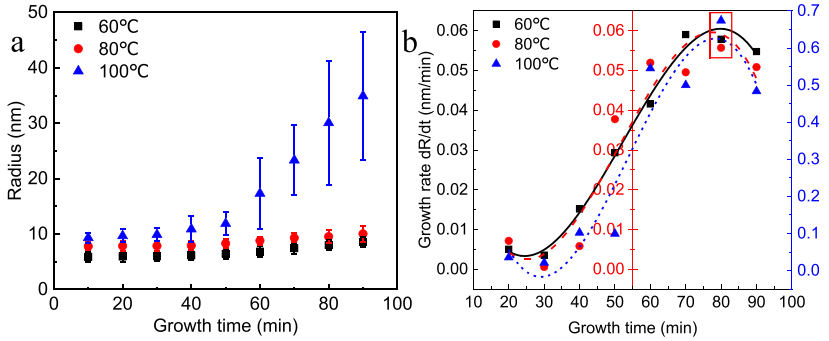

Figure 11. (a) Variations of HgSe QD size with growth time; (b) growth rate of HgSe QDs with the growth time.

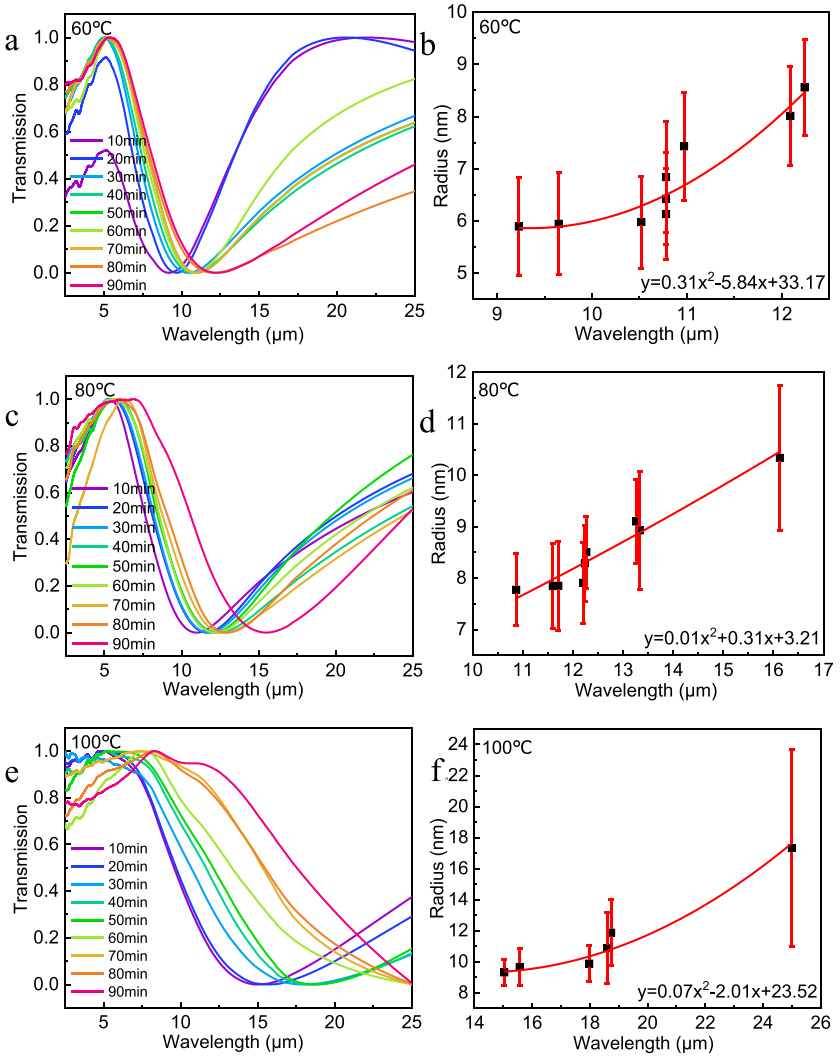

Figure 12. (a, c, e) Transmission spectra of HgSe QDs; (b, d, f) relationships between the radius of HgSe QDs and the characteristic peaks of the transmission spectra.

concentration of monomers decreased rapidly. When the monomer concentration was below the "nucleation threshold", the nucleation process ceased, and the remaining monomers in the solution began to "grow" on the crystal nucleus, which formed grains. With the increase of grains, when the monomer concentration continued to drop to a certain critical value, the Ostwald ripening phenomenon occurred.[25] This process continues until the dissolving monomer is in equilibrium with the monomer concentration around the grain. Therefore, the growth rate in Figure 10 will eventually drop to 0 nm/min as the growth time increases, at which point the size distribution will be more uniform. The variations of QD size and growth rate with growth time at different temperatures are shown in Figure 11a,b.

As can be seen from Figure 11, the QD size increased with the reaction temperature when the growth time was consistent. Also, the longer the growth time, the faster the QD size increase. It can be seen from Figure 11b that the growth rates of QDs all changed in the S-shaped curve. The growth rate was the

https://doi.org/10.1021/acsomega.3c05910
ACS Omega 2023, 8, 44804−44811

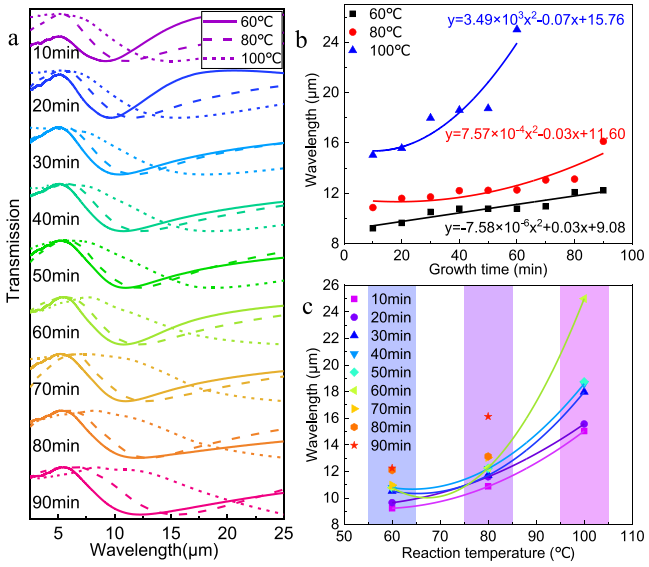

Figure 13. (a) Infrared transmission spectra of HgSe QDs at different temperatures and different growth times; (b) fitting curves of the characteristic peak with growth time; (c) fitting curves of the characteristic peak with reaction temperature.

minimum at 30 min, reached the maximum at 80 min, and would eventually drop to 0 nm/min. The maximum growth rate was 0.06 nm/min and was basically unchanged when the reaction temperature was less than 80 °C. The maximum growth rate increased to 10 times, which was 0.63 nm/min when the temperature reached 100 °C.

3.2.2. The Characterization of FTIR. The transmission spectra of HgSe QDs synthesized at different growth times and reaction temperatures are shown in Figure 12a,c,e. The relationships between the radius of HgSe QDs and the characteristic peaks of transmission spectra are shown in Figure 12b,d,f. The original data are shown in Table S3 (Supporting Information).

It can be seen from Figure 12a,c,e and Table S3 that the transmission peaks of HgSe QDs gradually red-shift with the increase in growth time. The characteristic peak red-shifted from 9.23 to 12.24 μm when the reaction temperature was 60 °C. The characteristic peak red-shifted from 10.87 to 16.13 μm when the reaction temperature was 80 °C. Also, the characteristic peak red-shifted from 15.04 μm to the far-infrared band when the reaction temperature was 100 °C (the furthest measured by the spectrometer is only 25 μm). It can be seen from Figure 12b–f that the radius of HgSe QDs and the characteristic peaks of transmission spectra showed nonlinear positive correlation, which accords with the quantum confinement effect.

The infrared transmission spectra of HgSe QDs at different temperatures and different growth times are shown in Figure 13. The fitting curves of the characteristic peak with growth time are shown in Figure 13b. The fitting curves of the characteristic peak with reaction temperature are shown in Figure 13c.

It can be seen from Figure 13a,b that the characteristic peak of QDs would red-shift with the increase in reaction temperature when the growth time of QDs was the same. Also, the higher the reaction temperature, the faster the red-shift speed. The variation of the spectral peak was consistent with the size of the QDs, which accords with the quantum confinement effect.

As can be seen from Figure 13c, the red-shift rate of the characteristic peak was slow when the growth time was 10–20 min, the red-shift rate was increased when the growth time was 30–50 min, and the infrared characteristic peak of the QDs has exceeded the detection range when the reaction temperature was 100 °C and the growth time was greater than 50 min, but it can be seen from the trend that the red-shift rate will be more rapidly increased with the increase in temperature.

The characterization of EDS is revealed in the Supporting Information.

4. CONCLUSIONS

The HgSe QDs were synthesized by a hot injection. The effects of materials ratio, growth time, and reaction temperature on the growth and spectral properties of HgSe QDs were studied by TEM, STEM, SEM, EDS, XRD, and FTIR characterization.

The following conclusions have been obtained from the experimental results:

First of all, the excess SeS_2 would be reduced to the crystallized or incompletely crystallized Se elementary substance with the increase in SeS_2 in the ratio of materials. The particle size of the reduced Se element increased with the content of SeS_2. Then, since the growth of QDs is competitive with that of Se elements, too much SeS_2 is not conducive to the growth of HgSe QDs, and the content and particle size of HgSe QDs in the product decreased with SeS_2. In addition, the best raw material ratio was obtained to get the highest QDs content, and the yield was up to 53.04% when the molar ratio of $Hg(OAc)_2$ to SeS_2 was 1:1.5.

After that, the adhesion and separation rate of ligands on the surface of nanocrystals was accelerated with the increase in growth time and reaction temperature, and the average size of the QDs gradually increased, forming a polyhedron with a thermodynamically stable surface. The critical radii of QDs were 7.91, 9.40, and 26.92 nm at the reaction temperatures of 60, 80, and 100 °C, respectively. Also, the growth rates of QDs all changed in the S-shaped curve, and the growth rate was the minimum at 30 min, reached the maximum at 80 min, and would eventually drop to 0 nm/min. When the reaction temperature was less than 80 °C, the maximum growth rate was 0.06 nm/min and was basically unchanged. When the temperature reached 100 °C, the maximum growth rate increased to 10 times, which was 0.63 nm/min. Furthermore, the transmission peak of HgSe QDs would red-shift with the increase in growth time, and the red-shift rate can be accelerated by increasing the reaction temperature.

■ ASSOCIATED CONTENT

Supporting Information

The Supporting Information is available free of charge at https://pubs.acs.org/doi/10.1021/acsomega.3c05910.

Effect of precursor ratio on HgSe QDs (characterization of XRD and EDS) and effect of growth time and reaction temperature on HgSe QDs (characterization of XRD, FTIR, and EDS) (PDF)

■ AUTHOR INFORMATION

Corresponding Authors

Tengxiao Guo − *State Key Laboratory of NBC Protection for Civilian, Beijing 102205, China*; Email: guotengxiao@sklnbcpc.cn

https://doi.org/10.1021/acsomega.3c05910
ACS Omega 2023, 8, 44804−44811

Shuya Cao − *State Key Laboratory of NBC Protection for Civilian, Beijing 102205, China*; Email: caoshuya@sklnbcpc.cn

Author

Suhui Wang − *State Key Laboratory of NBC Protection for Civilian, Beijing 102205, China*; orcid.org/0009-0002-0525-3632

Complete contact information is available at: https://pubs.acs.org/10.1021/acsomega.3c05910

Author Contributions

S.W.: methodology, validation, investigation, and writing of the original draft; T.G.: review and editing; S.C.: supervision and review and editing. All authors have read and agreed to the published version of the manuscript.

Funding

This work is funded by the National Key R&D Program of China (2021YFC3330201).

Notes

The authors declare no competing financial interest.

■ ACKNOWLEDGMENTS

The authors thanks Hangzhou Yanqu Information Technology Co., Ltd., for technical support in SEM and XRD testing. The authors also thanks Shanghai WEIPU Testing Technology Group Co., Ltd., for technical support in TEM testing.

■ REFERENCES

(1) Howes, P.; Green, M.; Johnston, C.; et al. Synthesis and shape control of mercury selenide (HgSe) quantum dots [J]. *J. Mater. Chem.* **2008**, *18* (29), 3474.

(2) Deng, Z.; Jeong, K. S.; Guyot-Sionnest, P. Colloidal Quantum Dots Intraband Photodetectors. *ACS Nano* **2014**, *8*, 11707.

(3) Deng, Z.; Guyot-Sionnest, P. Intraband Luminescence from HgSe/CdS Core/Shell Quantum Dots [J]. *ACS Nano* **2016**, *10* (2), 2121.

(4) Lhuillier, E.; Scarafagio, M.; et al. Infrared Photodetection Based on Colloidal Quantum-Dot Films with High Mobility and Optical Absorption up to THz[J]. *Nano Lett.* **2016**, *16*, 1282−1286.

(5) Jana, M. K.; Chithaiah, P.; Murali, B.; et al. Near infrared detectors based on HgSe and HgCdSe quantum dots generated at the liquid-liquid interface [J]. *Journal of Materials Chemistry C* **2013**, *1* (39), 6184−6187.

(6) Lhuillier, E.; Guyot-Sionnest, P. Recent Progresses in Mid Infrared Nanocrystal Optoelectronics. *IEEE J. Sel. Top. Quantum Electron.* **2017**, *23* (5), 1.

(7) Livache, C.; Martinez, B.; Goubet, N.; et al. A colloidal quantum dot infrared photodetector and its use for intraband detection. *Nat. Commun.* **2019**, *10*, 10.

(8) Tang, X.; Wu, G. F.; Lai, K. W. C. Plasmon resonance enhanced colloidal HgSe quantum dot filterless narrowband photodetectors for mid-wave infrared [J]. *Journal of Materials Chemistry C* **2017**, *5* (2), 362−369.

(9) Xiong, Q.; Chowdhury, F. I.; Wang, X. Filter-Free Narrowband Photodetectors Employing Colloidal Quantum Dots. *IEEE J. Sel. Top. Quantum Electron.* **2018**, *24* (2), 1.

(10) Zhao, X.; Mu, G.; Tang, X.; et al. Mid-IR Intraband Photodetectors with Colloidal Quantum Dots. *Coatings* **2022**, *12* (4), 467.

(11) Wang, L. *Synthesis of Mid-Infrared HgSe Quantum Dots and Study of Their Film Properties [M]*. HeNan University, 2022, 6.

(12) Zhang, H. Y.; Hu, Z. Q.; Lu, K. Transformation from the amorphous to the nanocrystalline state in pure selenium. *Nanostruct. Mater.* **1995**, *44* (1), 41−114.

(13) Wang, L.; Niu, M.-G.; Wu, Z.-W.; Yang, S.-M. Preparation and Characterization of Single Crystal Se Nanowires. *J. Xinyang Norm. Univ.* **2009**, *22* (1), 92−94.

(14) Gates, B.; Mayers, B.; Cattle, B.; Xia, Y. Synthesis and Characterization of Uniform Nanowires of Trigonal Selenium. *Adv. Funct. Mater.* **2002**, *12* (3), 219−227.

(15) Li, Q.; Yam, V. W. High-yield synthesis of selenium nanowires in water at room temperature *Chem. Commun.* **2006** 9 1006 1008DOI: .

(16) Ma, Y. Q. L.; Ma, J.; Cheng, H. Micelle-Mediated Synthesis of Single-Crystalline Selenium Nanotubes. *Adv. Mater.* **2004**, *16* (12), 1023−1026.

(17) Barns, R. L. A Method of Preparation of Powder Samplas for DebyeScherrer-Hull X-ray Diffraction [J]. *Journal of applied crystallography* **1972**, *5*, 381.

(18) Jiang, Z.; Xie, S.; Zhang, X.; et al. High Purity Trigonal Selenium Nanorods Growth via Laser Ablation Under Controlled Temperature [J]. *Chem. Phys. Lett.* **2003**, *368*, 425−429.

(19) Wang, X.; Zheng, X.; Lu, J.; Xie, Y. Reduction of selenious acid induced by ultrasonic irradiation−−formation of Se nanorods. *Ultrason. Sonochem.* **2004**, *11* (5), 307−310.

(20) Mokari, T.; Zhang, M.; Yang, P. Shape, Size, and Assembly Control of PbTe Nanocrystals. *J. Am. Chem. Soc.* **2007**, *129*, 9864−9865.

(21) Li, G.; Wang, H.; Zhang, T.; et al. Solvent-Polarity-Engineered Controllable Synthesis of Highly Fluorescent Cesium Lead Halide Perovskite Quantum Dots and Their Use in White Light-Emitting Diodes [J]. *Adv. Funct. Mater.* **2016**, *26* (46), 8478−8486.

(22) Xie, T.; Zhuang, Z.; Liu, L.; et al. Shape Control of CdSe Nanocrystals with Zinc Blende Structure. *J. Am. Chem. Soc.* **2009**, *131* (45), 16423−16429.

(23) Murray, C. B.; Kagan, C. R.; Bawendi, M. G. Synthesis and Characterization of Monodisperse Nanocrystals and Close-Packed Nanocrystal Assemblies [J]. *Annu. Rev. Mater. Sci.* **2000**, *30*, 545−610.

(24) Lamer, V. K.; Dinegar, R. H. Theory, Production and Mechanism of Formation of Monodispersed Hydrosols [J]. *J. Am. Chem. Soc.* **1950**, *72* (11), 4847−4854.

(25) Voorhees, P. W. The Theory of Ostwald Ripening [J]. *J. Stat. Phys.* **1985**, *38*, 231−252.